# A Gut-Brain Axis-on-a-Chip for studying transport across epithelial and endothelial barriers

Min-Hyeok Kim<sup>1</sup>, Donghyun Kim<sup>2</sup>, and Jong Hwan Sung<sup>1</sup>

<sup>1</sup>Hongik University <sup>2</sup>Yonsei University

February 25, 2021

# Abstract

Recent research on Gut-Brain Axis (GBA) has suggested that the gut luminal environment, including the dietary components and commensal microbiota, could affect behavior, emotion, and cognitive abilities in the brain. The research on GBA has heavily relied on animal models, which makes the research challenging. Recent advances in organ-on-a-chip technology could be a solution for GBA research. In present work, we developed a modular microfluidic chip, where gut epithelial and brain endothelial cells were co-cultured to form the gut epithelial barrier and the Blood-Brain Barrier (BBB). Cell responses to microbial byproducts were examined by TEER measurement for each barrier, and we observed the transport of fluorescently labeled exosome across the gut barrier towards the BBB. Our results suggest this model can be used as a novel in vitro model of GBA for studying the interaction between the gut and the brain.

# 1. Introduction

A considerable number of studies have suggested the existence of so-called Gut-Brain Axis (GBA), indicating that the gut environment could affect the neurocognitive functions of the brain (Dinan & Cryan, 2017; Iannone et al., 2019). For example, an increase in intestinal permeability may induce systemic immune dysregulation, resulting in neuroinflammation (Gorecki, Dunlop, Rodger, & Anderton, 2020), or changes in the dietary pattern contribute to psychiatric conditions by altering the gut microbiota composition (Sandhu et al., 2017). These responses can be mediated by microbiome-produced molecules entering systemic circulation across the gut, yet it remains unclear whether these molecules reach brain sites directly or only induce central responses via long-distance neural signaling (Martin, Osadchiy, Kalani, & Mayer, 2018).

Due to its complexity, studies on GBA have mainly relied on *in vivo* animal models (Raimondi et al., 2020). They require experienced animal handling (Maheshwari et al., 2018), feature poor experimental reproducibility (Voelkl et al., 2020), and real-time sensing of responses is difficult (Zhang, Korolj, Lai, & Radisic, 2018). Moreover, extrapolation of animal data to humans could be problematic, leading to an increased need for in vitro experimental model for GBA research. Recent advances in organ-on-a-chip technologies could be a solution for such problems (Ma, Peng, Li, & Chen, 2020; Wang et al., 2020). Organ-on-a-chip is a technology that can simulate the physiological environment and functionality of human organs on a chip to mimic the key organotypic cellular architecture and functionality, 3D extracellular matrix, biochemical factors, and biophysical cues at a smaller scale (S. H. Lee & J. H. Sung, 2018; Sung et al., 2018).

It is thought that the gut and the brain communicate via multiple pathways, and one of the routes is based on the passage of soluble microbial-derived products from the microbiota across the gut epithelium and the blood-brain barrier (BBB) to reach the brain cells, (Raimondi et al., 2020). The gut epithelium protects the systemic circulation from harmful xenobiotic compounds, and the BBB plays a vital role in maintaining the physical and chemical homeostasis of the brain and protects the brain from harmful molecules and pathogens in the blood (Jiang, Li, Zheng, Li, & Huang, 2019; Sharma et al., 2019; Shimizu, Nishihara, & Kanda, 2018). Some gut environment-originated substrates or membrane vesicles such as exosomes may travel via the bloodstream to the BBB, and eventually exert an influence on the brain (Fig. 1) (Evrensel & Ceylan, 2015; Haas-Neill & Forsythe, 2020; Lauritzen et al., 2014; McAllister et al., 2001; Parker, Fonseca, & Carding, 2020).

In present work, we developed a modular GBA chip based on our previous Gut-Liver chips (Lee, Ha, Choi, & Sung, 2017; S. Y. Lee & J. H. Sung, 2018). This microfluidic device consists of two parts which are gut barrier module (upper part) and BBB module (bottom part) (Fig. 2). We observed of changes in barriers via measurement of trans-endothelial/epithelial electrical resistance (TEER) and examined the delivery of exosomes across the gut barrier to the BBB. As there is a lack of in vitro models for the investigation of inter-organ communication of gut and brain (Wang et al., 2020), our device could give a chance to understand this complex system.

## 2. Materials & Methods

# 2.1. Fabrication of microfluidic chip

The master molds were 3D-printed using Anycubic Photon LCD printer (China). Then, the molds were coated using trichloro (1H,1H,2H,2H-perfluorooctyl) silane (Sigma, USA, 448931). 2 ml of this coating agent was co-incubated with the molds in a vacuum desiccator overnight. Chips were composed of polydimethyl-siloxane (PDMS; Dow Corning, USA, 761036). PDMS prepolymer solution was mixed with the curing agent at 10:1 ratio, poured onto molds or square dishes, and cured at 60 for 6 h. Cured PMDS parts were assembled (Fig. 2). The membrane for cell culture area was polyester membranes cut from transwell inserts with 0.4 µm pore size (Corning, USA, 3470).

## 2.2. Cell preparation and culture

We used human gut epithelial cell line (Caco-2; ATCC, USA, HTB-37), murine brain endothelial cell line (bEnd.3; ATCC, USA, CRL-2299), and primary human brain microvascular endothelial cells (hBMECs; Cell Systems, USA, ACBRI 376). The two cell lines were cultured using Dulbecco's Modified Eagle Medium (DMEM; Gibco, USA, 11965118) supplemented with 10% fetal bovine serum (FBS; ScienCell, USA, 0500) and 1% Penicillin/Streptomycin (P/S; ScienCell, USA, 0513). The hBEMCs were cultured using endothelial cell medium (ECM; ScienCell, USA, 1001) supplemented with 5% FBS, 1% P/S and 1% endothelial cell growth supplement (ECGS; ScienCell, USA, 1052). All cell types were incubated in humidified atmosphere of 5% CO<sub>2</sub> at 37 during flask culture and chip experiment. Cell culture media were changed every 2-3 days.

# 2.3. Cell seeding and co-culture on the chip and wells

The upper gut barrier module has  $0.2 \times 0.2$  mm channel size,  $0.5 \text{ cm}^2$  cell culture area and capacity of 0.6 ml medium. The bottom BBB module has  $0.3 \times 0.3$  mm channel size,  $0.28 \text{ cm}^2$  cell culture area and capacity of 0.85 ml medium. A 96 well plate (Corning, USA, 3988) and 24 transwell plate (Corning, USA, 3470) were used for control experiment. Each well of 96 well plate contains 0.3 ml of medium, each apical chamber of 24 well plate contains 0.2 ml of medium, and each basal chamber of 24 well plate contains 1 ml of medium.

The brain endothelial cell line was used first to optimize initial seeding condition for later experiments using hBMECs. Caco-2 was suspended in 0.1 ml of medium at  $2 \times 10^6$  cells/ml density to be seeded at  $4 \times 10^5$  cells/cm<sup>2</sup> on upper module, cultured for 5 days until cells completely cover the membrane, and exposed to fluidic flow for next 5 days. 2 days after Caco-2 was exposed to the flow, either bEnd.3 or hBMECs was were suspended in 0.056 ml of medium at  $3 \times 10^5$  cells/ml density to be seeded at  $6 \times 10^4$  cells/cm<sup>2</sup> on each bottom module. After culturing the endothelial cells for 3 days, the modules were assembled and co-cultured under flow condition for 24h. For control experiment, gut cells and brain endothelial cells were cultured in wells at same cell density.

Lipopolysaccharide (LPS; Sigma, USA, L2637) and sodium butyrate (NaB; Sigma, USA, B5887) were chosen as a model toxin and a model drug. 100  $\mu$ g/ml of LPS was treated onto the gut in both well and chip while

brain endothelial cells in well were treated with 0.1  $\mu$ g/ml of LPS, for 24 hours in all cases. 2 mM of NaB was treated onto gut cells in the chip and 0.2 mM of NaB was treated onto brain endothelial cells in transwell for 24 hours.

#### 2.4. Measurement of TEER

TEER measurement was used to determine barrier integrity. TEER measurement for each module was conducted by a resistance-based method illustrated in Fig. 3A. This method was a four-point probe method like commonly used STX chopstick electrodes.

After co-culturing gut and BBB, the upper and bottom module were detached from each other. Then, resistance of each module was measured using Millicell ERS-2 Volt-Ohm meter (Millipore, USA, MERS00002). TEER of each barrier was determined from the resistance values using equation (1).

$$TEER = A * (R - R_{\text{blank}}) \tag{1}$$

A is cell culture area (cm<sup>2</sup>), R is resistance of module with cell layer ( $\Omega$ ) and R<sub>blank</sub> is resistance of module with no cell ( $\Omega$ ).

#### 2.5. Permeability assay

The permeability coefficient of each barrier was measured using FITC-dextran 3-5 kDa (Sigma, USA, FD4). The amount of FITC-dextran transported across the cell barrier was measured for 3 h with 1 h term. The permeability coefficient of each cell barrier was determined using equation (2).

$$P_{\rm app} = \frac{C}{t} \times \frac{V}{A * C_0} \tag{2}$$

 $P_{app}$  is permeability coefficient (cm/s), C is basolateral concentration (mg/ml), V is basolateral volume (ml), t is time (sec), A is cell culture area (cm<sup>2</sup>), and C<sub>0</sub> is initial apical concentration (mg/ml).

#### 2.6. IL-8 ELISA assay

Quantitation of pro-inflammatory cytokine interlukin-8 (IL-8) was performed using Duoset ELISA kit (R&D Systems, USA, DY208). Caco-2 and hBMECs were cultured in GBA chip and 96 well. Each well used for culturing contained 0.3 ml of medium. Media obtained from the chip and wells with Caco-2 were diluted to 1/3 concentration while those from wells with hBMECs were diluted to 1/100 concentration. The assay followed the user manual. Briefly, 96 well used for the assay was pre-coated with capture antibody. Then, sample media were added into each pre-coated well and incubated. Sample was removed from each well, and then detection antibodies are added and incubated. Next, the antibodies were removed and streptavidin-HRP was added. After incubation avoiding direct light, streptavidin-HRP was removed, extract solution was added and incubated. Finally, stop solution was added to stop further reaction and absorbance of each well was measured using an UV-VIS spectrometer (Multiskan GO; Thermofisher, USA, N10588).

#### 2.7. Cell staining

Live/Dead staining assay was conducted to determine viability of cultured cells. Calcein AM (Invitrogen, USA, C34852) and ethidium homodimer-1 (Invitrogen, USA, E1169) were diluted to 4  $\mu$ M and 2  $\mu$ l of each solution was added into 1 ml of phosphate-buffered saline (PBS; Sigma, USA, P3813). Cells were incubated with Live/Dead solution for 90 min. F-actin and nucleus were stained to assess formation of cell monolayer. First, cells were fixed by 4% paraformaldehyde (Sigma, USA, 8187081000) for 10 min. Next, fixed tissue was treated with 0.5% Triton-X 100 (JUNSEI, Japan, 49415-1601) for 3 min. Then, the tissue was stained by FITC-phalloidin (Sigma, USA, P5282) and 0.1  $\mu$ g/ml of DAPI (Sigma, USA, 10236276001) for 30 and 1 min respectively. The Images were taken by a fluorescence microscope (Olympus, Japan, CKX41) or a confocal microscope (Carl Zeiss, Germany, LSM 880).

#### 2.8. Exosome isolation, labeling, and treatment

FBS contained in the complete DMEM was replaced with exosome-depleted FBS (Gibco, USA, A2720803) to isolate cell-derived exosomes without bovine exosome. Then, Caco-2 cells at 70-90% confluency in flask were cultured with this exosome-free medium. Three days later, the media were collected from the flasks to isolate exosomes. Exosomes were isolated using Total Exosome Isolation Reagent (Invitrogen, USA, 4478359) following the user manual. The isolated exosomes were suspended in PBS and fluorescence-labeled by 18:1 PE-TopFluor® AF488 (Avanti® Polar Lipid, UAA, 810386C). Before the labeling, exosomes in PBS were counted using EXOCET Exosome Quantitation Kit (System Biosciences, USA, EXOCET96A-1) following the user manual. Exosomes at  $4 \times 10^8$  particles/ml were directly treated into the mono-cultured BBB for 2 h. Exosomes at  $8 \times 10^8$  particles/ml were treated into the gut barrier module of GBA chip for 6 h.

# 2.9. Fluid dynamics simulation

Shear stress profiles on chip were simulated using COMSOL Multiphysics software (Comsol Inc., Sweden). Initial flow velocity at the channel entrance were assumed to be 4.26 mm/s and 9.66 mm/s for the gut barrier module and the BBB module respectively, based on the measurement of volume flow rate.

# 2.10. Statistical analysis

Difference in mean between two independent groups was tested using Student's t-test. Results of all experiments were collected from at least 3 independent experiments for each sample. Data shown in the bar graph was presented as mean +/- standard deviation (SD).

# 3. Results & Discussion

## 3.1. Chip fabrication and TEER measurement in the chip

The overall design of the GBA chip was based on our previous gut-liver chip models (Lee et al., 2017; S. Y. Lee & J. H. Sung, 2018). The GBA chip consists of two parts, gut barrier module and BBB module, which can be easily assembled and separated (Fig. 2). Each module has channels to provide fluidic flow (Shemesh et al., 2015), and porous membranes to support cell culture and reproduce the barrier function of corresponding tissues.

In a microfluidic chip, the current distribution through the cell layer determines TEER measurement accuracy and is affected by membrane area, probe design/shape, and microfluidic channel geometry (ávan der Meer, JungáKim, ávan der Helm, & den Berg, 2015; Elbrecht, Long, & Hickman, 2016). The measured TEER values of both cells in the chip showed similar values to those of transwell counterparts (Fig. 3). TEER values of Caco-2 and bEnd.3 were between 220 and 230  $\Omega^* \text{cm}^2$  and approximately 20  $\Omega^* \text{cm}^2$ respectively, for both chip and static well cultures, consistent with previously reported values. The range of TEER values for Caco-2 was reported to be 100-200  $\Omega^* \text{cm}^2$  and that of bEnd.3 ranged from 15 to 30  $\Omega^* \text{cm}^2$ (Booth & Kim, 2012; Chi et al., 2015; S. Y. Lee & J. H. Sung, 2018; Puscas et al., 2019).

#### 3.2. Shear stress & Cell culture

The spatial distribution of shear stress levels inside the chip was predicted by COMSOL Multiphysics simulation. The predicted values of shear stress in the gut barrier module ranged between  $0.04 \times 10^{-4}$  and  $1.33 \times 10^{-4}$  dyne/cm<sup>2</sup> (Fig. 4A).. The shear stress levels within *in vivo* small intestine are known to be approximately  $2.2 \times 10^{-7}$  dyne/cm<sup>2</sup> (Choe, Ha, Choi, Choi, & Sung, 2017). Although our shear stress in the gut barrier module was higher than that *in vivo*, Caco-2 cells formed confluent cell layer when co-cultured with the brain endothelial cells (Fig. 5A and 5D). Several gut-on-a-chip studies have reported shear stress higher than in vivo values (Chi et al., 2015; Choe et al., 2017; Kim, Huh, Hamilton, & Ingber, 2012), where the Caco-2 layers got reliable integrity, promoting Caco-2 differentiation (Ashammakhi et al., 2020).

The predicted shear stress levels in the BBB module were  $0.01 \times 10^{-3} - 1.22 \times 10^{-3}$  dyne/cm<sup>2</sup> in the BBB module (Fig. 4B). In contrast, shear stress levels within the brain microvasculature range from 4 to 20 dyne/cm<sup>2</sup> (Colgan et al., 2007). Many studies have been conducted at shear stress levels lower than the reported *in* 

vivo range, and were able to achieve reliable barrier formation (Oddo et al., 2019). In our study, the brain endothelial cells showed high survival rate with confluent cell layer when co-cultured with Caco-2 (Fig. 5B, 5C, 5E and 5F). Our results show that our GBA chip can support co-culture of gut epithelial and blood endothelial cells.

### 3.3. LPS-induced changes in gut barrier and BBB

To simulate the inflammatory response of gut-brain axis, our GBA chip was treated with LPS. The TEER values of the gut and the BBB were decreased in response to LPS treatment, with increased permeability of both barriers (Fig. 6A<sup>-</sup>D). LPS can be found on the cell walls of Gram-negative bacteria (Schumann, 1992), which is known to disrupt gut integrity and can penetrate systemic circulation across the gut barrier (Ghosh, Wang, Yannie, & Ghosh, 2020; Hirotani et al., 2008). This endotoxin can also impair BBB integrity and increased circulating LPS is associated with brain-related issues (Banks & Erickson, 2010; Qin et al., 2007; Zhu et al., 2017). Although the gut epithelium and BBB showed a similar trend in overall, the extent of response to LPS was different depending on the culture condition. For example, both cells seemed less sensitive to LPS in transwell condition than chip condition. In chip condition, physiological properties of Caco-2 such as barrier function, absorptive property and enzyme activity can be altered (Choe et al., 2017), which suggests that the response of Caco-2 cells to LPS may be affected by the flow.

It is also notable that the changes in absorption permeability was more significant than the changes in TEER in response to LPS. In the gut chip developed by Chi et al., Caco-2 cells featured 0.9 fold change in TEER and 2 fold change in permeability when exposed to flow (Chi et al., 2015). In the study conducted by Hirotani et al., a similar trend was observed, where the absorption permeability changed more dramatically than the values of TEER (Hirotani et al., 2008). The TEER value reflects the ionic conductance of the paracellular pathway in the cell monolayer while the flux of non-electrolyte tracers represents the paracellular water flow and the pore size of the tight junctions (Srinivasan et al., 2015). As TEER and flux of non-electrolyte tracers indicate different entities, the change in TEER value does not always correspond to the change in permeability of paracellular pathway (Zucco et al., 2005).

A proinflammatory cytokine, IL-8 is thought to engage in several inflammatory processes (Ehrlich et al., 1998), and BBB could be a crucial source of them, which could influence brain microenvironment (Banks & Erickson, 2010; Chen et al., 2001; Verma, Nakaoke, Dohgu, & Banks, 2006). The bEnd.3 cell line used in our study is a murine cell line, which shows inflammatory response different from human cells (Asfaha et al., 2013). Therefore, we used the primary human brain microvascular endothelial cell, hBMECs, to study inflammatory response in our GBA chip (Fig  $6E^{-}G$ ). The IL-8 assay was conducted to confirm if proper alteration in the cytokine secretion can be observed after the endotoxin stimulation in the gut. Caco-2 cells in the well did not show significant changes. In contrast, hBMECs in the well showed significant increase of the cytokine after the stimulation. This result implies that the hBMECs were more sensitive to LPS treatment and the induced inflammatory response observed in our GBA chip originate mostly from brain endothelial cells.

# 3.4. Butyrate-induced changes in the integrity of gut and BBB

We studied the effect of sodium butyrate (NaB) on the gut epithelium and BBB (Fig. 7). When NaB was applied to the gut barrier module, the integrity of both gut barrier and BBB was improved, judging from the increase in the measured TEER values. hBMECs mono-cultured in transwell was directly exposed to NaB and showed increased TEER value. Given these results, we speculate that NaB treated in the gut exerted a positive effect on the brain endothelium. Butyrate is known to enhance barrier function of gut epithelium and thought to be important in maintaining the gut health (Bedford & Gong, 2018; L. Peng, He, Chen, Holzman, & Lin, 2007). Also, it has been reported that butyrate affect BBB permeability and exerts neuroprotective effect by restoring the BBB (Braniste et al., 2014; Li et al., 2016). Preserving and restoring BBB integrity presents a primary target for developing neuroprotective strategies (Parker et al., 2020), suggesting this short-chain fatty acids (SCFA) can be a drug candidate targeting GBA. Our study has demonstrated that the modular GBA chip can recapitulate the beneficial effect of NaB via interaction

with gut epithelium and BBB.

#### 3.5. Transport of exosomes across the gut epithelium to the BBB

Exosomes are known to move across gut epithelium or BBB (Carobolante, Mantaj, Ferrari, & Vllasaliu, 2020; Saeedi, Israel, Nagy, & Turecki, 2019), and several animal studies imply they play important roles in affecting the cognitive ability (Manca et al., 2018; Mutai, Zhou, & Zempleni, 2017; Zempleni, Sukreet, Zhou, Wu, & Mutai, 2019). Furthermore, exosomes in the blood stream showed natural brain targeting ability (H. Peng et al., 2020). The transport of fluorescence-labeled exosomes across the gut epithelium and BBB was examined in our GBA chip (Fig. 8). In case of the co-culture, uptake of exosomes by the gut layer under flow condition was not significantly affected, while the BBB took up more exosome uptake by the mono-cultured hBMECs. Taking these results together, it seems that the fluidic condition enhances exosome transport across the gut epithelium, and uptake by the brain endothelial cells. Iason et al. assessed uptake and translocation of angiopoietin-2-modified liposomes in their BBB chip (Papademetriou, Vedula, Charest, & Porter, 2018), and more Ang2-liposomes were transported across the BBB with increasing fluidic shear. Our results also suggest that the fluidic shears stress can affect the exosome translocation across the gut epithelium.

## 4. Conclusion

To the best of our knowledge, only few GBA-on-a-chip models have been reported to date. Herein, a prototypic GBA-on-a-chip was suggested, where gut and BBB were co-cultured. Responses of cells to microbial substrates correlated with *in vivo* models. We also assessed transport of exosomes in the GBA chip, suggesting the fluidic environment caused changes in the transport of exosomes. There should exist multiple direct/indirect pathways where microbial products and exosomes in the gut affect the brain. To uncover these pathways, inclusion of microbiome, gut cells, immune cells, BBB and neurons in our GBA chip is desirable for future studies.

## 5. Acknowledgments

This work was supported by National Research Foundation of Korea, under Grant (Basic Research Lab, 2019R1A4A1025958), and by the Ministry of Trade, Industry & Energy (MOTIE), Republic of Korea, under the Technology Innovation Program, Grant 20008414 (Development of intestine-liver-kidney multiorgan tissue chip mimicking absorption distribution metabolism excretion of drug), and by the Hongik University Research Fund.

## Figures

Fig. 1 Schematics of Gut-Brain Axis (GBA). (A) Gut-BBB-Brain interaction. (B) Gut-Brain communication through blood stream. Created with BioRender.com.

Fig. 2 The design of GBA chip and the picture of assembled GBA chip (A) Cross-sectional view of assembled chip. (B) Schematics of of each module. (C) Image of the assembled chip.

Fig. 3 The scheme of TEER measurement in the chip. (A) Illustrations on TEER measurement. Comparison of TEER value between static chip-cultured cells and transwell-cultured cells for (B) gut barrier module and (C) BBB module. NS: Not significant; p>0.05, Student's t-test (n=3).

Fig. 4 COMSOL Multiphysics simulation of fluidic shear stress inside the GBA chip. Simulation for (A) gut barrier module and (B) BBB module.

Fig. 5 Fluorescent images of cells seeded in the chip. Live/daed Images of (A) Caco-2, (B) bEnd.3, and (C) hBMECs when co-cultured (green=live, red=dead). F-actin/nucleus stain images of (D) Caco-2 cells, (E) bEnd.3 cells and (F) hBMECs when co-cultured (blue=nucleus, green=F-actin).

Fig. 6 LPS-induced changes in co-culture chip and mono-culture transwell. Changes in Caco-2 barrier represented as (A) TEER and (B) permeability coefficient. Changes in bEnd.3 barrier represented as (C) TEER and (D) permeability coefficient. Changes in cytokine secretion of (E) Caco-2-hBMECs co-culture chip, (F) Caco-2 mono-cultured in the well and (G) hBMECs mono-cultured in the well. NS: Not significant; p>0.05, \*\*p<0.01, \*\*\*p<0.001, Student's t-test (n[?]3).

Fig. 7 Changes in barrier functions of cells by butyrate in chips and wells. Changes in TEER value of (A) Caco-2 co-cultured in chip, (B) hBMECs co-cultured in chip and (C) hBMECs mono-cultured in transwell. NaB : Sodium butyrate, NS: Not significant; p>0.05, \*\*p<0.01, \*\*\*p<0.001, Student's t-test (n[?]3).

Fig. 8 Exosome delivery to BBB across gut barrier in the co-culture chip. (A) co-cultured gut epithelium, (B) co-cultured brain endothelium (C) mono-cultured brain endothelium in the absence of flow (blue=nucleus, green=exosome). (D) co-cultured gut epithelium, (E) co-cultured brain endothelium and (F) mono-cultured brain endothelium in the presence of flow (blue=nucleus, green=exosome). Quantitative comparison of exosome uptake with presence or absence of flow on (G) co-cultured gut epithelium, (H) co-cultured brain endothelium and (I) mono-cultured brain endothelium. NS: Not significant; p>0.05, p<0.05, Student's t-test (n=3)

## References

avan der Meer, A. D., JungaKim, H., avan der Helm, M. W., & den Berg, A. (2015). Measuring direct current trans-epithelial electrical resistance in organ-on-a-chip microsystems. *Lab on a Chip*, 15 (3), 745-752.

Asfaha, S., Dubeykovskiy, A. N., Tomita, H., Yang, X., Stokes, S., Shibata, W., . . . Muthupalani, S. (2013). Mice that express human interleukin-8 have increased mobilization of immature myeloid cells, which exacerbates inflammation and accelerates colon carcinogenesis. *Gastroenterology*, 144 (1), 155-166.

Ashammakhi, N., Nasiri, R., De Barros, N. R., Tebon, P., Thakor, J., Goudie, M., . . . Khademhosseni, A. (2020). Gut-on-a-chip: Current progress and future opportunities. *Biomaterials*, 120196.

Banks, W. A., & Erickson, M. A. (2010). The blood-brain barrier and immune function and dysfunction. *Neurobiology of disease*, 37 (1), 26-32.

Bedford, A., & Gong, J. (2018). Implications of butyrate and its derivatives for gut health and animal production. *Animal Nutrition*, 4 (2), 151-159.

Booth, R., & Kim, H. (2012). Characterization of a microfluidic in vitro model of the blood-brain barrier (µBBB). Lab on a Chip, 12 (10), 1784-1792.

Braniste, V., Al-Asmakh, M., Kowal, C., Anuar, F., Abbaspour, A., Tóth, M., . . . Kundu, P. (2014). The gut microbiota influences blood-brain barrier permeability in mice. *Science translational medicine*, 6 (263), 263ra158-263ra158.

Carobolante, G., Mantaj, J., Ferrari, E., & Vllasaliu, D. (2020). Cow Milk and Intestinal Epithelial Cell-Derived Extracellular Vesicles as Systems for Enhancing Oral Drug Delivery. *Pharmaceutics*, 12 (3), 226.

Chen, P., Shibata, M., Zidovetzki, R., Fisher, M., Zlokovic, B., & Hofman, F. (2001). Endothelin-1 and monocyte chemoattractant protein-1 modulation in ischemia and human brain-derived endothelial cell cultures. *Journal of neuroimmunology*, 116 (1), 62-73.

Chi, M., Yi, B., Oh, S., Park, D.-J., Sung, J. H., & Park, S. (2015). A microfluidic cell culture device ( $\mu$ FCCD) to culture epithelial cells with physiological and morphological properties that mimic those of the human intestine. *Biomedical microdevices*, 17 (3), 58.

Choe, A., Ha, S. K., Choi, I., Choi, N., & Sung, J. H. (2017). Microfluidic Gut-liver chip for reproducing the first pass metabolism. *Biomedical microdevices*, 19 (1), 4.

Colgan, O. C., Ferguson, G., Collins, N. T., Murphy, R. P., Meade, G., Cahill, P. A., & Cummins, P. M. (2007). Regulation of bovine brain microvascular endothelial tight junction assembly and barrier function by laminar shear stress. *American Journal of Physiology-Heart and Circulatory Physiology*, 292 (6), H3190-H3197.

Dinan, T. G., & Cryan, J. F. (2017). Brain-gut-microbiota axis—mood, metabolism and behaviour. *Nature Reviews Gastroenterology & Hepatology*, 14 (2), 69-70.

Ehrlich, L. C., Hu, S., Sheng, W. S., Sutton, R. L., Rockswold, G. L., Peterson, P. K., & Chao, C. C. (1998). Cytokine regulation of human microglial cell IL-8 production. *The Journal of Immunology*, 160 (4), 1944-1948.

Elbrecht, D. H., Long, C. J., & Hickman, J. J. (2016). Transepithelial/endothelial Electrical Resistance (TEER) theory and ap-plications for microfluidic body-on-a-chip devices. tc, 1 (1), 1.

Evrensel, A., & Ceylan, M. E. (2015). The gut-brain axis: the missing link in depression. *Clinical Psychopharmacology and Neuroscience*, 13 (3), 239.

Ghosh, S. S., Wang, J., Yannie, P. J., & Ghosh, S. (2020). Intestinal barrier dysfunction, LPS translocation, and disease development. *Journal of the Endocrine Society*, 4 (2), bvz039.

Gorecki, A. M., Dunlop, S. A., Rodger, J., & Anderton, R. S. (2020). The gut-brain axis and gut inflammation in Parkinson's disease: stopping neurodegeneration at the toll gate: Taylor & Francis.

Haas-Neill, S., & Forsythe, P. (2020). A Budding Relationship: Bacterial Extracellular Vesicles in the Microbiota–Gut–Brain Axis. International Journal of Molecular Sciences, 21 (23), 8899.

Hirotani, Y., Ikeda, K., Kato, R., Myotoku, M., Umeda, T., Ijiri, Y., & Tanaka, K. (2008). Protective effects of lactoferrin against intestinal mucosal damage induced by lipopolysaccharide in human intestinal Caco-2 cells. *Yakugaku Zasshi*, 128 (9), 1363-1368.

Iannone, L. F., Preda, A., Blottière, H. M., Clarke, G., Albani, D., Belcastro, V., . . . Ferraris, C. (2019). Microbiota-gut brain axis involvement in neuropsychiatric disorders. *Expert review of neurotherapeutics*, 19 (10), 1037-1050.

Jiang, L., Li, S., Zheng, J., Li, Y., & Huang, H. (2019). Recent progress in microfluidic models of the blood-brain barrier. *Micromachines*, 10 (6), 375.

Kim, H. J., Huh, D., Hamilton, G., & Ingber, D. E. (2012). Human gut-on-a-chip inhabited by microbial flora that experiences intestinal peristalsis-like motions and flow. *Lab on a Chip*, 12 (12), 2165-2174.

Lauritzen, K. H., Morland, C., Puchades, M., Holm-Hansen, S., Hagelin, E. M., Lauritzen, F., . . . Bergersen, L. H. (2014). Lactate receptor sites link neurotransmission, neurovascular coupling, and brain energy metabolism. *Cerebral cortex*, 24 (10), 2784-2795.

Lee, D. W., Ha, S. K., Choi, I., & Sung, J. H. (2017). 3D gut-liver chip with a PK model for prediction of first-pass metabolism. *Biomedical microdevices*, 19 (4), 1-13.

Lee, S. H., & Sung, J. H. (2018). Organ-on-a-chip technology for reproducing multiorgan physiology. Advanced healthcare materials, 7 (2), 1700419.

Lee, S. Y., & Sung, J. H. (2018). Gut-liver on a chip toward an in vitro model of hepatic steatosis. *Biotechnology and bioengineering*, 115 (11), 2817-2827.

Li, H., Sun, J., Wang, F., Ding, G., Chen, W., Fang, R., . . . Liu, J. (2016). Sodium butyrate exerts neuroprotective effects by restoring the blood-brain barrier in traumatic brain injury mice. *Brain research*, 1642, 70-78.

Ma, C., Peng, Y., Li, H., & Chen, W. (2020). Organ-on-a-Chip: A New Paradigm for Drug Development. *Trends in Pharmacological Sciences*.

Maheshwari, R., Gupta, A., Ganeshpurkar, A., Chourasiya, Y., Tekade, M., & Tekade, R. K. (2018). Guiding Principles for Human and Animal Research During Pharmaceutical Product Development *Dosage Form Design Parameters* (pp. 621-664): Elsevier. Manca, S., Upadhyaya, B., Mutai, E., Desaulniers, A. T., Cederberg, R. A., White, B. R., & Zempleni, J. (2018). Milk exosomes are bioavailable and distinct microRNA cargos have unique tissue distribution patterns. *Scientific reports*, 8 (1), 1-11.

Martin, C. R., Osadchiy, V., Kalani, A., & Mayer, E. A. (2018). The brain-gut-microbiome axis. *Cellular* and molecular gastroenterology and hepatology, 6 (2), 133-148.

McAllister, M. S., Krizanac-Bengez, L., Macchia, F., Naftalin, R. J., Pedley, K. C., Mayberg, M. R., . . . Janigro, D. (2001). Mechanisms of glucose transport at the blood-brain barrier: an in vitro study. *Brain research*, 904 (1), 20-30.

Mutai, E., Zhou, F., & Zempleni, J. (2017). Depletion of dietary bovine milk exosomes impairs sensorimotor gating and spatial learning in C57BL/6 mice. *The FASEB Journal*, 31 (1\_supplement), 150.154-150.154.

Oddo, A., Peng, B., Tong, Z., Wei, Y., Tong, W. Y., Thissen, H., & Voelcker, N. H. (2019). Advances in microfluidic blood-brain barrier (BBB) models. *Trends in biotechnology*, 37 (12), 1295-1314.

Papademetriou, I., Vedula, E., Charest, J., & Porter, T. (2018). Effect of flow on targeting and penetration of angiopep-decorated nanoparticles in a microfluidic model blood-brain barrier. *PloS one*, 13 (10), e0205158.

Parker, A., Fonseca, S., & Carding, S. R. (2020). Gut microbes and metabolites as modulators of blood-brain barrier integrity and brain health. *Gut Microbes*, 11 (2), 135-157.

Peng, H., Ji, W., Zhao, R., Yang, J., Lu, Z., Li, Y., & Zhang, X. (2020). Exosome: a significant nano-scale drug delivery carrier. *Journal of Materials Chemistry B*, 8 (34), 7591-7608.

Peng, L., He, Z., Chen, W., Holzman, I. R., & Lin, J. (2007). Effects of butyrate on intestinal barrier function in a Caco-2 cell monolayer model of intestinal barrier. *Pediatric research*, 61 (1), 37-41.

Puscas, I., Bernard-Patrzynski, F., Jutras, M., Lecuyer, M.-A., Bourbonniere, L., Prat, A., . . . Roullin, V. G. (2019). IVIVC Assessment of Two Mouse Brain Endothelial Cell Models for Drug Screening. *Pharmaceutics*, 11 (11), 587.

Qin, L., Wu, X., Block, M. L., Liu, Y., Breese, G. R., Hong, J. S., . . . Crews, F. T. (2007). Systemic LPS causes chronic neuroinflammation and progressive neurodegeneration. *Glia*, 55 (5), 453-462.

Raimondi, I., Izzo, L., Tunesi, M., Comar, M., Albani, D., & Giordano, C. (2020). Organ-on-a-chip in vitro models of the brain and the blood-brain barrier and their value to study the Microbiota-Gut-Brain Axis in neurodegeneration. *Frontiers in Bioengineering and Biotechnology*, 7, 435.

Saeedi, S., Israel, S., Nagy, C., & Turecki, G. (2019). The emerging role of exosomes in mental disorders. *Translational psychiatry*, 9 (1), 1-11.

Sandhu, K. V., Sherwin, E., Schellekens, H., Stanton, C., Dinan, T. G., & Cryan, J. F. (2017). Feeding the microbiota-gut-brain axis: diet, microbiome, and neuropsychiatry. *Translational Research*, 179, 223-244.

Schumann, R. (1992). Function of lipopolysaccharide (LPS)-binding protein (LBP) and CD14, the receptor for LPS/LBP complexes: a short review. *Research in immunology*, 143 (1), 11-15.

Sharma, G., Sharma, A. R., Lee, S.-S., Bhattacharya, M., Nam, J.-S., & Chakraborty, C. (2019). Advances in nanocarriers enabled brain targeted drug delivery across blood brain barrier. *International Journal of Pharmaceutics*, 559, 360-372.

Shemesh, J., Jalilian, I., Shi, A., Yeoh, G. H., Tate, M. L. K., & Warkiani, M. E. (2015). Flow-induced stress on adherent cells in microfluidic devices. *Lab on a Chip*, 15 (21), 4114-4127.

Shimizu, F., Nishihara, H., & Kanda, T. (2018). Blood-brain barrier dysfunction in immuno-mediated neurological diseases. *Immunological Medicine*, 41 (3), 120-128.

Srinivasan, B., Kolli, A. R., Esch, M. B., Abaci, H. E., Shuler, M. L., & Hickman, J. J. (2015). TEER measurement techniques for in vitro barrier model systems. *Journal of laboratory automation*, 20 (2), 107-126.

Sung, J. H., Wang, Y. I., Narasimhan Sriram, N., Jackson, M., Long, C., Hickman, J. J., & Shuler, M. L. (2018). Recent advances in body-on-a-chip systems. *Analytical chemistry*, 91 (1), 330-351.

Verma, S., Nakaoke, R., Dohgu, S., & Banks, W. A. (2006). Release of cytokines by brain endothelial cells: a polarized response to lipopolysaccharide. *Brain, behavior, and immunity, 20* (5), 449-455.

Voelkl, B., Altman, N. S., Forsman, A., Forstmeier, W., Gurevitch, J., Jaric, I., . . . Van de Casteele, T. (2020). Reproducibility of animal research in light of biological variation. *Nature Reviews Neuroscience*, 1-10.

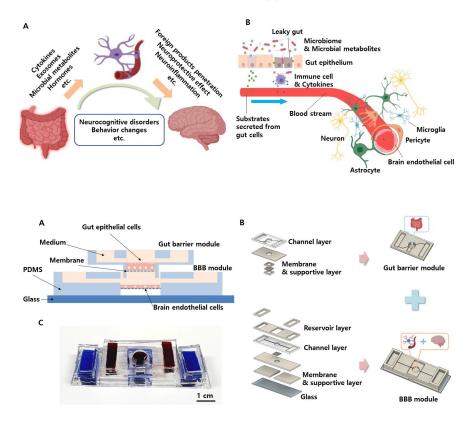
Wang, X., Hou, Y., Ai, X., Sun, J., Xu, B., Meng, X., . . . Zhang, S. (2020). Potential applications of microfluidics based blood brain barrier (BBB)-on-chips for in vitro drug development. *Biomedicine & Pharmacotherapy*, 132, 110822.

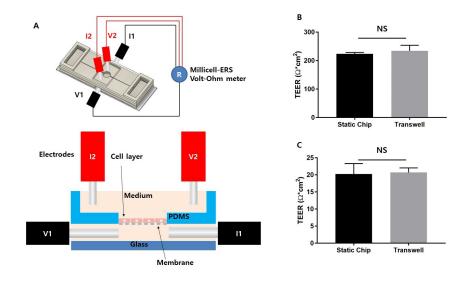
Zempleni, J., Sukreet, S., Zhou, F., Wu, D., & Mutai, E. (2019). Milk-derived exosomes and metabolic regulation. *Annual review of animal biosciences*, 7, 245-262.

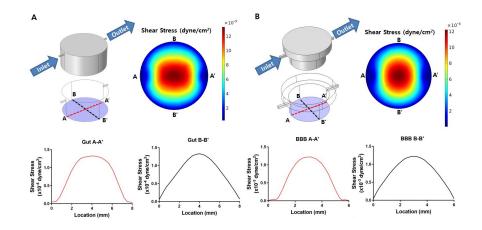
Zhang, B., Korolj, A., Lai, B. F. L., & Radisic, M. (2018). Advances in organ-on-a-chip engineering. *Nature Reviews Materials*, 3 (8), 257-278.

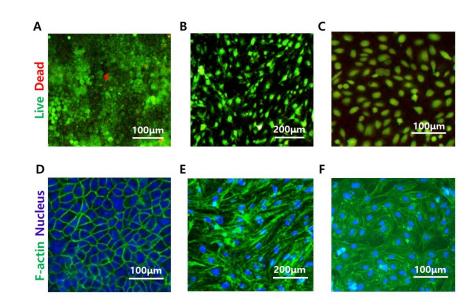
Zhu, X., Han, Y., Du, J., Liu, R., Jin, K., & Yi, W. (2017). Microbiota-gut-brain axis and the central nervous system. *Oncotarget*, 8 (32), 53829.

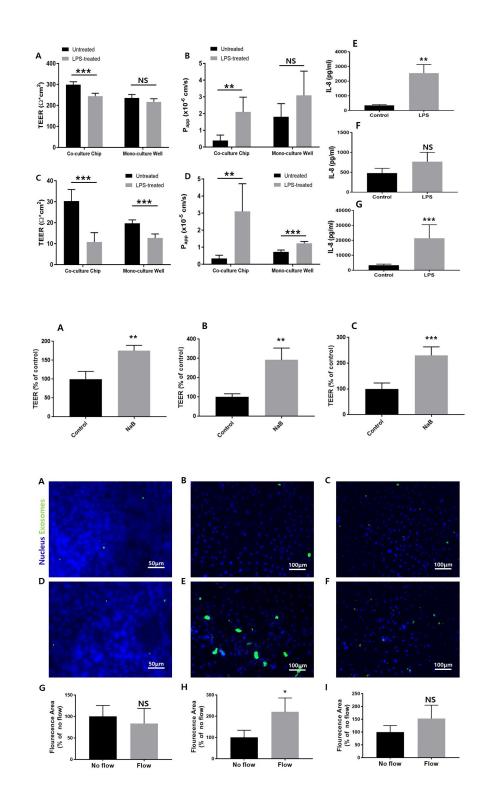
Zucco, F., Batto, A.-F., Bises, G., Chambaz, J., Chiusolo, A., Consalvo, R., . . . Fabre, G. (2005). An interlaboratory study to evaluate the effects of medium composition on the differentiation and barrier function of Caco-2 cell lines. *Alternatives to laboratory animals*, 33 (6), 603-618.











E.
relim
rel
e p
ð,
ma
8
Dai
wec
1e
revie
30 L
ě
een
<u>.</u>
no
as
and h
an
rint
epr
pre
3
his
Η.
Z
16
4751
6124
റ്
222
612
n.1
_a
225
01.0
ğ
https://
ĝ.
d.
ISSIO
rmission.
permissio
erm
hout perm
hout perm
without perm
without perm
reuse without perm
No reuse without perm
No reuse without perm
rved. No reuse without perm
reserved. No reuse without perm
reserved. No reuse without perm
rights reserved. No reuse without perm
rights reserved. No reuse without perm
All rights reserved. No reuse without perm
rights reserved. No reuse without perm
All rights reserved. No reuse without perm
/funder. All rights reserved. No reuse without perm
All rights reserved. No reuse without perm
author/funder. All rights reserved. No reuse without perm
author/funder. All rights reserved. No reuse without perm
/funder. All rights reserved. No reuse without perm
the author/funder. All rights reserved. No reuse without perm
the author/funder. All rights reserved. No reuse without perm
the author/funder. All rights reserved. No reuse without perm
ght holder is the author/funder. All rights reserved. No reuse without perm
ight holder is the author/funder. All rights reserved. No reuse without perm
ght holder is the author/funder. All rights reserved. No reuse without perm
ie copyright holder is the author/funder. All rights reserved. No reuse without perm
The copyright holder is the author/funder. All rights reserved. No reuse without perm
ie copyright holder is the author/funder. All rights reserved. No reuse without perm
- The copyright holder is the author/funder. All rights reserved. No reuse without perm
The copyright holder is the author/funder. All rights reserved. No reuse without perm
eb 2021 — The copyright holder is the author/funder. All rights reserved. No reuse without perm
Feb 2021 — The copyright holder is the author/funder. All rights reserved. No reuse without perm
25 Feb 2021 — The copyright holder is the author/funder. All rights reserved. No reuse without perm
orea 25 Feb 2021 — The copyright holder is the author/funder. All rights reserved. No reuse without perm
orea 25 Feb 2021 — The copyright holder is the author/funder. All rights reserved. No reuse without perm
ea 25 Feb 2021 — The copyright holder is the author/funder. All rights reserved. No reuse without perm
orea 25 Feb 2021 — The copyright holder is the author/funder. All rights reserved. No reuse without perm
Authorea 25 Feb 2021 — The copyright holder is the author/funder. All rights reserved. No reuse without perm